Isogeometric FEM Implementation of High-Order Surface Impedance Boundary Conditions

Rafael Vázquez[1], Annalisa Buffa[1], and Luca di Rienzo[2]

[1]Istituto di Matematica Applicata e Tecnologie Informatiche del CNR, Pavia I-27100, Italy
[2]Dipartimento di Elettronica, Informazione e Bioingegneria, Politecnico di Milano, Milan 20133, Italy

I. Introduction

SURFACE impedance boundary conditions (SIBCs), as introduced by Leontovich [2], have become a standard tool in computational electromagnetics. They offer the advantage that in the presence of conductors and under the condition of strong skin effect it is possible to solve the problem only outside the conductors, without having to resolve the boundary layer.

The low-order condition given by Leontovich only considers the local tangential plane over the surface of the conductor. Higher order conditions for smooth conductors were given by Rytov [3], on the basis of the principle of asymptotic expansions in terms of the skin depth. These conditions also consider the curvature of the surface of the conductor, and the tangential derivative of the field. For a further review on SIBCs we refer to [4] and [5]. The mathematical analysis of high-order SIBCs has been performed in [6] for scalar problems and in [7] for vectorial problems. In particular, the authors have proved the convergence of the SIBCs when the skin depth tends to zero.

In this paper, we introduce the different kinds of high-order SIBCs presented in [6] in a variational formulation to be discretized with Galerkin's method. We have chosen a 2-D formulation in terms of magnetic vector potential, as in [1] and [8], where the problem is discretized with the boundary element method (BEM). The variational formulation that we propose can be discretized with the finite element method (FEM). In this paper, however, we have decided to perform the numerical simulations using the isogeometric analysis (IGA) method [9]. This is a discretization technique based on nonuniform rational B-splines (NURBS), a set of functions which are widely used in computer aided design (CAD) software. One of the advantages of IGA in this context is that it allows for an efficient computation of the curvature of the boundary of the domain, which is required by high-order SIBCs.

Manuscript received June 20, 2013; revised September 9, 2013; accepted January 2, 2014. Date of publication January 23, 2014; date of current version June 6, 2014. Corresponding author: R. Vázquez (e-mail: vazquez@imati.cnr.it).

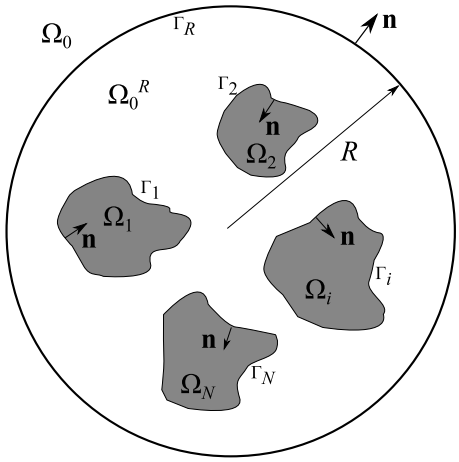

Fig. 1. Geometry of the problem.

The remainder of this paper is organized as follows. In Section II, we present the equations of the problem in terms of magnetic vector potential. Different SIBCs are given in Section III, and the variational formulation for each choice SIBC is introduced in Section IV. A brief introduction to IGA is presented in Section V, and the numerical results for several test cases are discussed in Section VI.

II. Magnetic Vector Potential Formulation

Consider a set of N infinitely long parallel conductors, with cross sections $\Omega_i, i = 1, \ldots, N$, and let us denote by $\Omega_0 \subset \mathbb{R}^2$ the surrounding air (see Fig. 1). Each conductor is assumed to have electrical conductivity σ_i, and magnetic permeability μ_i, with μ_0 the magnetic permeability of free space.

We consider a 2-D formulation of the time-harmonic eddy-current model, written in terms of the magnetic vector potential $\mathbf{A} = A\mathbf{e}_z$, as in [8]. Splitting the potential into "source" and "eddy" components, $A = A^s + A^e$, it can be seen that A^s is constant in each conductor, and we will denote by A^s_i its value in Ω_i. Denoting by A^e_{int} and A^e_{ext} the restriction of A^e to the conductors and to Ω_0, respectively, the 2-D problem inside the conductors reads

$$\nabla^2 A^e_{\text{int}} = j\omega\mu_i\sigma_i A^e_{\text{int}} \quad \text{in } \Omega_i, \quad i = 1, \ldots, N \tag{1}$$

and in the nonconducting domain

$$\nabla^2 A^e_{\text{ext}} = 0 \qquad \text{in } \Omega_0. \tag{2}$$

Denoting by Γ_i the boundary of (the cross section of) each conductor, and by $\mathbf{n}$ the unit normal vector exterior to Ω_0, the equations for A^e are completed with the interface conditions

$$A^e_{\text{int}} = A^e_{\text{ext}} - A^s_i \qquad \text{on } \Gamma_i \tag{3}$$

$$\frac{1}{\mu_i}\frac{\partial A^e_{\text{int}}}{\partial \mathbf{n}} = \frac{1}{\mu_0}\frac{\partial A^e_{\text{ext}}}{\partial \mathbf{n}} \qquad \text{on } \Gamma_i. \tag{4}$$

To avoid dealing with the infinite domain Ω_0, we follow a standard approach in finite elements: we truncate the domain far away from the conductors, and impose an absorbing boundary condition on the external boundary [10, Ch. 9]. Alternative approaches would be the use of perfectly matched layers (PML) [10, Ch. 9], infinite elements [11, Ch. 16], or a hybrid FEM-BEM method. Let us denote by Ω_0^R the intersection of Ω_0 with the circle of radius R, and by Γ_R its external boundary (see Fig. 1), where we apply the following second order absorbing boundary condition [12, Sec. 3.3]:

$$\frac{\partial A^e_{\text{ext}}}{\partial \mathbf{n}} + \frac{3A^e_{\text{ext}}}{8R} - \frac{1}{2R}\frac{\partial^2 A^e_{\text{ext}}}{\partial \xi^2} = 0 \qquad \text{on } \Gamma_R \tag{5}$$

where ξ denotes the curvilinear coordinate over the boundary contour.

Since the values of the source component A^s are unknown, we need one more condition on each conductor to complete the set of equations. This condition is the intensity flowing in each conductor

$$\int_{\Gamma_i} \frac{1}{\mu_0}\frac{\partial A^e_{\text{ext}}}{\partial \mathbf{n}}\, d\xi = I_i, \quad i = 1, \ldots, N. \tag{6}$$

III. Surface Impedance Boundary Conditions

The general idea of applying SIBCs is to replace the solution of the problem inside the conductor given by (1) with an approximate boundary condition on its boundary. The method is valid under the condition of skin effect, that is, in each conductor the penetration depth $\delta_i = \sqrt{2/\omega\mu_i\sigma_i}$ is much smaller than the characteristic size of the conductor cross section.

Defining $\alpha = \sqrt{2j}$, the first-order (Leontovich), second-order (Mitzner) and third-order (Rytov) SIBCs on Γ_i are, respectively [6], [8]

$$\frac{\partial A^e_{\text{int}}}{\partial \mathbf{n}} = \frac{-\alpha}{\delta_i} A^e_{\text{int}} \tag{7}$$

$$\frac{\partial A^e_{\text{int}}}{\partial \mathbf{n}} = \frac{-2\alpha^2}{\delta_i^2\kappa + 2\alpha\delta_i} A^e_{\text{int}} \tag{8}$$

$$\left(\frac{\delta_i}{\alpha} + \frac{\kappa\delta_i^2}{2\alpha^2} + \frac{3\kappa^2\delta_i^3}{8\alpha^3}\right)\frac{\partial A^e_{\text{int}}}{\partial \mathbf{n}} + \frac{\delta_i^3}{2\alpha^3}\frac{\partial^2}{\partial \xi^2}\left(\frac{\partial A^e_{\text{int}}}{\partial \mathbf{n}}\right) + A^e_{\text{int}} = 0 \tag{9}$$

where $\kappa = \kappa(\xi)$ is the (signed) curvature of the contour of the cross section.

As it is explained in [6], the conditions (7)–(9) are obtained through the approximation of a Neumann-to-Dirichlet (NtD) operator, that gives A^e_{int} as a function of the normal derivative $\partial A^e_{\text{int}}/\partial \mathbf{n}$. Alternative conditions are proposed in [6] by the approximation of a Dirichlet-to-Neumann (DtN) operator, which is the inverse of the NtD one. The first-order condition is the same as (7), since the first-order DtN and NtD approximation operators are inverse to each other. The same is not true for second- and third-order operators, and in this case the DtN conditions are, respectively

$$\frac{\partial A^e_{\text{int}}}{\partial \mathbf{n}} = \left(\frac{-\alpha}{\delta_i} + \frac{\kappa}{2}\right) A^e_{\text{int}} \tag{10}$$

$$\frac{\partial A^e_{\text{int}}}{\partial \mathbf{n}} = \left(\frac{-\alpha}{\delta_i} + \frac{\kappa}{2} + \frac{\delta_i\kappa^2}{8\alpha}\right) A^e_{\text{int}} + \frac{\delta_i}{2\alpha}\frac{\partial^2 A^e_{\text{int}}}{\partial \xi^2}. \tag{11}$$

As we will see, the unknowns in the variational formulations are the fields A^e_{ext} and A^s_i. Hence, it is necessary to rewrite the SIBCs (7)–(11) in terms of those fields, by using the interface conditions (3)–(4). For instance, dividing (7) by μ_i and applying the interface conditions, we get

$$\frac{1}{\mu_0}\frac{\partial A^e_{\text{ext}}}{\partial \mathbf{n}} = \frac{1}{\mu_i}\frac{\partial A^e_{\text{int}}}{\partial \mathbf{n}} = \frac{-\alpha}{\mu_i\delta_i} A^e_{\text{int}} = \frac{-\alpha}{\mu_i\delta_i}(A^e_{\text{ext}} - A^s_i). \tag{12}$$

A similar procedure can be used for conditions (8)–(11).

In [6], the authors study the convergence properties of all these conditions when $\delta \to 0$ from a mathematical perspective. However, the choice of the most suitable SIBC may depend on the problem and also on the numerical method of discretization. One of the goals of this paper is to compare the effectiveness of these SIBCs, by performing numerical tests with a Galerkin discretization of the problem.

IV. Variational Formulation

In this section, we present the variational formulation of our problem applying the SIBCs presented above. In the first part of this section, we introduce the formulation for the low-order SIBC (7). After that, we present the formulation for all the high-order SIBCs, which are all very similar, except for condition (9). The variational formulation for this condition requires the use of an extra unknown for the normal derivatives, and it is presented at the end of this section. We remark that these formulations are valid in general for any Galerkin discretization method, and they can be discretized for instance with the standard FEM, or with IGA, as we will present in the next section. We also notice that, since we are focusing on the implementation, we do not write the problem in terms of sesquilinear forms, as it is done in [6] for the mathematical analysis of the problem.

A. Variational Formulation for Low-Order SIBC

Dividing (2) by μ_0, then multiplying by a test function v, and integrating over Ω_0^R, we obtain, after integrating by parts

$$\int_{\Omega_0^R} \frac{1}{\mu_0}\nabla A^e_{\text{ext}} \cdot \nabla v\, dS - \int_{\Gamma_R} \frac{1}{\mu_0}\frac{\partial A^e_{\text{ext}}}{\partial \mathbf{n}} v\, d\xi - \sum_{i=1}^{N} \int_{\Gamma_i} \frac{1}{\mu_0}\frac{\partial A^e_{\text{ext}}}{\partial \mathbf{n}} v\, d\xi = 0.$$

The integral on the external boundary Γ_R can be modified using the absorbing boundary condition (5). This yields, after integrating by parts the term with the second derivative

$$\frac{1}{\mu_0}\left(\int_{\Omega_0^R}\nabla A^e_{\text{ext}}\cdot\nabla v\,dS+\frac{1}{2R}\int_{\Gamma_R}\frac{\partial A^e_{\text{ext}}}{\partial\xi}\frac{\partial v}{\partial\xi}\,d\xi + \frac{3}{8R}\int_{\Gamma_R}A^e_{\text{ext}}v\,d\xi\right)-\sum_{i=1}^{N}\int_{\Gamma_i}\frac{1}{\mu_0}\frac{\partial A^e_{\text{ext}}}{\partial\mathbf{n}}v\,d\xi=0. \tag{13}$$

The integrals on Γ_i are transformed by applying (12), i.e., the SIBC expressed in terms of A^e_{ext} and A^s_i, to obtain

$$\frac{1}{\mu_0}\left(\int_{\Omega_0^R}\nabla A^e_{\text{ext}}\cdot\nabla v\,dS+\frac{1}{2R}\int_{\Gamma_R}\frac{\partial A^e_{\text{ext}}}{\partial\xi}\frac{\partial v}{\partial\xi}\,d\xi + \frac{3}{8R}\int_{\Gamma_R}A^e_{\text{ext}}v\,d\xi\right)+\sum_{i=1}^{N}\int_{\Gamma_i}\frac{\alpha}{\mu_i\delta_i}(A^e_{\text{ext}}-A^s_i)v\,d\xi=0. \tag{14}$$

Now, to write the formulation in a simpler and more convenient way, we define the operators

$$a(u,v):=\frac{1}{\mu_0}\left(\int_{\Omega_0^R}\nabla u\cdot\nabla v\,dS+\frac{1}{2R}\int_{\Gamma_R}\frac{\partial u}{\partial\xi}\frac{\partial v}{\partial\xi}\,d\xi+\frac{3}{8R}\int_{\Gamma_R}uv\,d\xi\right)$$

$$a_L(u,v)=\sum_{i=1}^{N}\int_{\Gamma_i}\frac{\alpha}{\mu_i\delta_i}uv\,d\xi$$

and we also define, for a vector of constants $\mathbf{C}=\{C_i\}_{i=1}^N\in\mathbb{C}^N$, the operator

$$b_L(v,\mathbf{C})=\sum_{i=1}^{N}\int_{\Gamma_i}\frac{\alpha}{\mu_i\delta_i}C_i v\,d\xi.$$

With these definitions, and introducing the vector of unknown sources $\mathbf{A}^s=\{A^s_i\}_{i=1}^N$, the variational formulation after applying the SIBC (7) becomes

$$a(A^e_{\text{ext}},v)+a_L(A^e_{\text{ext}},v)-b_L(v,\mathbf{A}^s)=0. \tag{15}$$

Equation (6) must be added to the system to make it solvable in the unknowns A^e_{ext} and $\mathbf{A}^s$. The condition is modified using (12), to give

$$\int_{\Gamma_i}\frac{1}{\mu_0}\frac{\partial A^e_{\text{ext}}}{\partial\mathbf{n}}\,d\xi=\int_{\Gamma_i}\frac{-\alpha}{\mu_i\delta_i}(A^e_{\text{ext}}-A^s_i)\,d\xi=I_i. \tag{16}$$

B. Variational Formulation for High-Order SIBCs

The variational formulations for the SIBCs (8), (10), and (11) are very similar to the one presented and can be obtained using the same procedure. Indeed, it is sufficient to replace a_L and b_L in (15) with similar operators, defined using the corresponding SIBC. For instance, the operator a_L should be replaced by

$$a_M(u,v)=\sum_{i=1}^{N}\int_{\Gamma_i}\frac{1}{\mu_i}\frac{2\alpha^2}{\delta_i^2\kappa+2\alpha\delta_i}uv\,d\xi \tag{17}$$

$$a_{M_{DtN}}(u,v)=\sum_{i=1}^{N}\int_{\Gamma_i}\frac{1}{\mu_i}\frac{2\alpha-\kappa\delta_i}{2\delta_i}uv\,d\xi \tag{18}$$

$$a_{R_{DtN}}(u,v)=\sum_{i=1}^{N}\int_{\Gamma_i}\frac{1}{\mu_i}\left(\frac{\alpha}{\delta_i}-\frac{\kappa}{2}-\frac{\delta_i\kappa^2}{8\alpha}\right)uv\,d\xi+\sum_{i=1}^{N}\int_{\Gamma_i}\frac{\delta_i}{2\mu_i\alpha}\frac{\partial u}{\partial\xi}\frac{\partial v}{\partial\xi}\,d\xi \tag{19}$$

when using (8), (10), and (11), respectively. The definition of the operators that replace b_L is very similar. Notice that since they are applied to constants, the derivatives when using condition (11) in this last operator are always zero.

As before, the intensity condition (6) must be added to the system. Applying the SIBCs (8), (10), and (11), it becomes, respectively

$$\int_{\Gamma_i}\frac{-2\alpha^2}{\mu_i(\delta_i^2\kappa+2\alpha\delta_i)}(A^e_{\text{ext}}-A^s_i)\,d\xi=I_i \tag{20}$$

$$\int_{\Gamma_i}\frac{1}{\mu_i}\left(\frac{-\alpha}{\delta_i}+\frac{\kappa}{2}\right)(A^e_{\text{ext}}-A^s_i)\,d\xi=I_i \tag{21}$$

$$\int_{\Gamma_i}\frac{1}{\mu_i}\left(\frac{-\alpha}{\delta_i}+\frac{\kappa}{2}+\frac{\delta_i\kappa^2}{8\alpha}\right)(A^e_{\text{ext}}-A^s_i)\,d\xi=I_i. \tag{22}$$

C. Variational Formulation for Rytov's NtD Condition

The formulation for the third-order SIBC (9) can be obtained with a mixed formulation, as it is done in [6]. The procedure is similar to the one explained in [10, Ch. 9] for third-order absorbing boundary conditions. The same approach has been used in [13] for high-order transmission conditions, in a discretization of vector fields.

We first introduce the new unknown $\varphi=\partial A^e_{\text{int}}/\partial\mathbf{n}$, that will replace the partial derivative in (6) and (13), using the interface condition (4), and also in the SIBC (9). Multiplying the latter by a test function ψ and integrating over Γ_i, then integrating by parts the term with the second partial derivative, and finally applying the interface condition (3), we get

$$\frac{\delta_i^3}{2\mu_i\alpha^3}\int_{\Gamma_i}\frac{\partial\varphi}{\partial\xi}\frac{\partial\psi}{\partial\xi}\,d\xi-\int_{\Gamma_i}\frac{1}{\mu_i}\left(\frac{\delta_i}{\alpha}+\frac{\kappa\delta_i^2}{2\alpha^2}+\frac{3\kappa^2\delta_i^3}{8\alpha^3}\right)\varphi\psi\,d\xi-\int_{\Gamma_i}\frac{1}{\mu_i}A^e_{\text{ext}}\psi\,d\xi+\int_{\Gamma_i}\frac{1}{\mu_i}A^s_i\psi\,d\xi=0. \tag{23}$$

To simplify the notation, for functions ϕ,ψ defined on the boundaries Γ_i where the SIBC is applied, and for a vector of

constants $\mathbf{C} = \{C_i\}_{i=1}^N \in \mathbb{C}^N$, we define the operators

$$\begin{aligned} c_R(\phi, \psi) &= \sum_{i=1}^{N} \frac{\delta_i^3}{2\mu_i \alpha^3} \int_{\Gamma_i} \frac{\partial \phi}{\partial \xi} \frac{\partial \psi}{\partial \xi}\, d\xi \\ &\quad - \int_{\Gamma_i} \frac{1}{\mu_i} \left(\frac{\delta_i}{\alpha} + \frac{\kappa \delta_i^2}{2\alpha^2} + \frac{3\kappa^2 \delta_i^3}{8\alpha^3} \right) \phi \psi \, d\xi \\ b_R(u, \psi) &= \sum_{i=1}^{N} \int_{\Gamma_i} \frac{1}{\mu_i} u \psi \, d\xi \\ d_R(\psi, \mathbf{C}) &= \sum_{i=1}^{N} \int_{\Gamma_i} \frac{1}{\mu_i} \psi C_i \, d\xi. \end{aligned} \tag{24}$$

Using the definition of these operators in (13) and (23), and replacing $\partial A^e_{\text{int}}/\partial \mathbf{n}$ by φ, the variational formulation is written as

$$\begin{aligned} a(A^e_{\text{ext}}, \upsilon) - b_R(\upsilon, \varphi) &= 0 \\ -b_R(A^e_{\text{ext}}, \psi) + c_R(\varphi, \psi) + d_R(\psi, \mathbf{A}^s) &= 0. \end{aligned} \tag{25}$$

As before, the system must be completed with the intensity condition (6), which in this case is written in terms of the new unknown φ, in the form

$$\int_{\Gamma_i} \frac{1}{\mu_i} \varphi \, d\xi = I_i, \quad i = 1, \ldots, N.$$

Remark 1: In the case of a multiconductor cable with a shield, like the third test in Section VI, two approaches are possible: to solve (1) in the shield, maintaining the absorbing boundary condition on Γ_R; or to impose a SIBC on the shield, as it is done in [14], and in practice truncating the computational domain in the internal boundary of the shield. Notice that in this case it is not necessary to impose the intensity across the shield, since the variational formulation guarantees that it is equal to $-\sum_{i=1}^N I_i$, as can be seen by taking the test function υ as a constant.

V. Isogeometric Analysis

Since the variational formulations of the previous section consider the curvature of the conductors, an efficient discretization with FEM is only possible with second (or higher)-order isoparametric finite elements [10, Ch. 4], or with curved finite elements. In this paper, we have chosen to discretize the problem with the IGA method. With this technique NURBS basis functions, which are utilized by the CAD software to describe the geometry, are also used as the shape functions in the discrete problem by invoking the isoparametric concept. As a result, the geometry description is done with NURBS, and an efficient and stable computation of the curvature is possible everywhere. This is in contrast with isoparametric elements, for which the curvature is not well defined between two elements. Moreover, in the IGA method it is possible to compute with high-degree and high-regularity basis functions, which gives similar approximation properties than FEM using less degrees of freedom. Finally, we remark that for the extension to the vectorial 3-D case, isogeometric curl-conforming spaces have been defined in [15].

In this section, we present a brief description of NURBS basis functions and the IGA method. For a deeper study on NURBS we refer the reader to the book [16], whereas for a more-detailed explanation of IGA we refer to the seminal paper [17] and the book [9].

A. NURBS Functions and Geometry

Univariate B-spline basis functions of degree p are defined from a nondecreasing knot vector $\Xi = \{0 = \zeta_1, \ldots, \zeta_{n+p+1} = 1\}$. We will only consider the case of open knot vectors, that is, the first $p+1$ knots are all equal to zero, and the last $p+1$ are all equal to one. Starting from piecewise constant functions

$$B_{k,0}(\zeta) = \begin{cases} 1, & \text{if } \zeta_k \le \zeta < \zeta_{k+1} \\ 0, & \text{otherwise} \end{cases}$$

B-splines of degree p are computed using the Cox-De Boor recursion formula

$$B_{k,p}(\zeta) = \frac{\zeta - \zeta_k}{\zeta_{k+p} - \zeta_k} B_{k,p-1}(\zeta) + \frac{\zeta_{k+p+1} - \zeta}{\zeta_{k+p+1} - \zeta_{k+1}} B_{k+1,p-1}(\zeta).$$

The resulting B-splines form a basis of the space of piecewise polynomials of degree p with $p - m_k$ continuous derivatives at the knot ζ_k, where m_k is the multiplicity of ζ_k. Some fundamental properties of B-splines are that they are non-negative, the basis function $B_{k,p}$ is supported in the interval $[\zeta_k, \zeta_{k+p+1})$, and on each knot span $[\zeta_k, \zeta_{k+1})$ there are at most $p+1$ non-null B-spline basis functions.

NURBS basis functions are defined as rational B-splines by associating a positive weight to each B-spline function, in the form

$$\hat{N}_{k,p}(\zeta) = \frac{w_k B_{k,p}(\zeta)}{\sum_{j=1}^n w_j B_{j,p}(\zeta)}. \tag{26}$$

NURBS basis functions inherit most of the properties of B-splines, in particular those related to their continuity and support.

Bivariate B-splines and NURBS are simply defined from the univariate ones by tensor product (see [16, Ch. 3]). For simplicity we maintain the same notation for univariate and bivariate functions.

A NURBS surface (respectively, curve) can be constructed by associating a control point $\mathbf{C_k} \in \mathbb{R}^2$ to each bivariate (respectively, univariate) basis function. This gives a parametrization of the form

$$\mathbf{F}(\boldsymbol{\zeta}) := \sum_{k=1}^{n} \hat{N}_{k,p}(\boldsymbol{\zeta}) \mathbf{C}_k, \quad \boldsymbol{\zeta} = (\zeta_1, \zeta_2) \in (0,1)^2. \tag{27}$$

The grid formed by the set of control points is usually called the control net, and it is one of the tools used in CAD software to manipulate the geometry (see Fig. 2). We remark that the parametrization of the boundary of the domain can be also written as a NURBS, using univariate basis functions and the control points on the boundary of the control net.

Several algorithms for the computation of NURBS basis functions and their derivatives, and also for the evaluation of the parametrization $\mathbf{F}$, can be found in [16]. In particular, the knot insertion and degree elevation algorithms recompute the

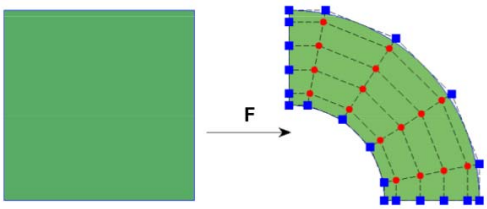

Fig. 2. Parametrization of one quarter of a ring using NURBS. Dashed lines: control net. Red dots: internal control points. Blue squares: boundary control points.

control points of the parametrization (27) when more knots are inserted (h-refinement) or the degree of the basis functions is raised (p-refinement).

In practice, complicated geometries cannot be given as the image of the unit square, like in (27), but as several patches that must be glued together. We give more details about this in Section V-C.

B. Isogeometric Analysis Based on NURBS

The idea behind IGA is to maintain the description of the geometry given as a NURBS, and to use the same NURBS basis functions for the discretization of the PDE problem. Let us assume that the domain Ω_0 is described with a NURBS parametrization like (27). Invoking the isoparametric concept, we look for a discrete solution of our problem in the form

$$A^e_{\text{ext}}(\mathbf{x}) = \sum_{k=1}^{n} A^e_k N_k(\mathbf{x}) \tag{28}$$

with N_k the basis functions in the physical domain, defined as

$$N_k(\mathbf{x}) = \hat{N}_k(\mathbf{F}^{-1}(\mathbf{x})). \tag{29}$$

Notice that, by the isoparametric approach, the degrees of freedom are in a one-to-one correspondence with the control points that define the parametrization (27). Compared with FEM, IGA can give more regular-basis functions, with up to $p-1$ continuous derivatives. Moreover, knot insertion and degree elevation algorithms allow us to refine the discrete space without modifying the original geometry.

It is also important to note that, since we are using open knot vectors [16, Ch 2], the only basis functions that do not vanish on the boundary are those associated to the control points on the boundary of the control net, marked as blue dots in Fig. 2. This can be seen in Fig. 3, where we depict a boundary and an internal basis function.

1) Discrete Problem for Low-Order SIBC: As for the variational formulation, we start describing how to compute the solution using the low-order condition (7), that is, we discretize the variational problem (15). In this case, the unknowns of our discrete problem are the vector of coefficients $\mathbf{A} = \{A^e_k\}_{k=1}^n$, and the value of the source component A^s in each conductor, that we represent with the vector $\mathbf{A}^s = \{A^s_i\}_{i=1}^N$. As in FEM, the solution within IGA is computed using a Galerkin method. Introducing the vector of intensities $\mathbf{I} = \{I_i\}_{i=1}^N$, the unknowns are computed by solving the linear system

$$\begin{bmatrix} \mathbf{K}+\mathbf{S} & -\mathbf{B}^\top \\ -\mathbf{B} & \mathbf{C} \end{bmatrix} \begin{bmatrix} \mathbf{A} \\ \mathbf{A}^s \end{bmatrix} = \begin{bmatrix} \mathbf{0} \\ \mathbf{I} \end{bmatrix} \tag{30}$$

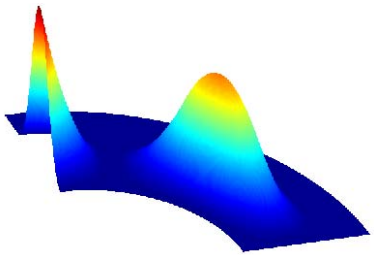

Fig. 3. Representation of two basis functions in the physical domain, one associated to a boundary control point, and one associated to an internal control point.

where the coefficients of the matrices $\mathbf{K} = [K_{kl}]$, $\mathbf{S} = [S^L_{kl}]$ and $\mathbf{B} = [B^L_{ik}]$ are given by

$$K_{kl} = a(N_k, N_l), k, l = 1, \ldots, n \tag{31}$$

$$S^L_{kl} = a_L(N_k, N_l), k, l = 1, \ldots, n \tag{32}$$

$$B^L_{ik} = \int_{\Gamma_i} \frac{\alpha}{\mu_i \delta_i} N_k \, d\xi, \quad i = 1, \ldots, N, \ k = 1, \ldots, n \tag{33}$$

with N_k the NURBS basis functions defined in (29). We remark that, although we are writing the equations for all the basis functions, the boundary integrals for (32) and (33) only have to be computed for the basis functions that do not vanish on the boundary. The second row of the system comes from the intensity condition (16), and $\mathbf{C}$ is a diagonal matrix with coefficients given by

$$C^L_{ii} = \int_{\Gamma_i} \frac{\alpha}{\mu_i \delta_i} \, d\xi.$$

2) Discrete Problem for High-Order SIBCs: The discrete version of the problem when applying the SIBCs (8), (10) or (11) can be written in the form (30), changing the matrices coefficients according to the SIBC. In fact, the matrix $\mathbf{K}$ is independent of the SIBC, with the same coefficients given in (31). The entries of $\mathbf{S}$ are computed replacing in (32) the operator a_L with the operator in (17)–(19) that corresponds to the desired SIBC. The coefficients of the matrix $\mathbf{B}$ and the diagonal matrix $\mathbf{C}$ are computed using (20)–(22).

3) Discrete Problem for Rytov's NtD Condition: As we have seen in Section IV, the variational formulation for Rytov's condition (9) requires us to introduce an extra unknown for the normal derivative. In the discrete setting, in addition to the discretization of A^e_{ext} given in (28), we need a discretization of the normal derivative $\varphi = \partial A^e_{\text{int}}/\partial \mathbf{n}$, that is only defined on the boundary.

As we mentioned, the boundary of the domain can be written as a univariate NURBS, using the control points on the boundary of the control net, and their associated basis functions. Denoting these basis functions by N^b_l, the discrete version of φ is very similar to (28) and takes the form

$$\varphi = \sum_{l=1}^{n_b} \varphi_l N^b_l \tag{34}$$

with n_b being the number of boundary basis functions.

Introducing the vector of unknown coefficients $\boldsymbol{\varphi} = \{\varphi_l\}_{l=1}^{n_b}$, the solution to the problem is computed by solving the linear

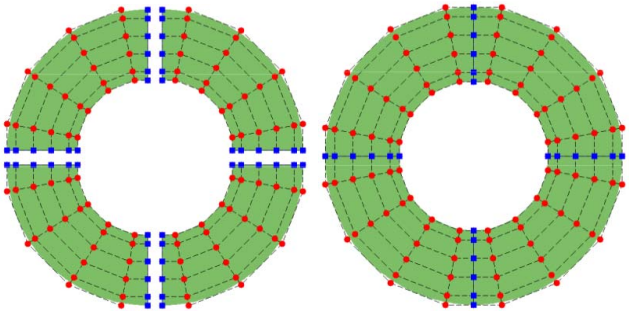

Fig. 4. Representation of a ring using four different NURBS patches (left). The control points at the interfaces between patches, represented by blue squares, must be coincident (right).

system

$$\begin{bmatrix} \mathbf{K} & -\mathbf{B}^\top & \mathbf{0} \\ -\mathbf{B} & \mathbf{C} & \mathbf{D}^\top \\ \mathbf{0} & \mathbf{D} & \mathbf{0} \end{bmatrix} \begin{bmatrix} \mathbf{A} \\ \boldsymbol{\varphi} \\ \mathbf{A}^s \end{bmatrix} = \begin{bmatrix} \mathbf{0} \\ \mathbf{0} \\ \mathbf{I} \end{bmatrix}. \tag{35}$$

The entries of the matrix $\mathbf{K}$ are the same given in (31). The coefficients of the matrices $\mathbf{B} = [B^R_{kl}]$, $\mathbf{C} = [C^R_{kl}]$, and $\mathbf{D} = [D^R_{ik}]$ can be derived from (24)

$$B^R_{kl} = b_R(N_k, N^b_l), \quad k = 1, \ldots, n, \ l = 1, \ldots, n_b$$
$$C^R_{kl} = c_R(N^b_k, N^b_l), \quad k, l = 1, \ldots, n_b$$
$$D^R_{ik} = \int_{\Gamma_i} \frac{1}{\mu_i} N^b_k \, d\xi \quad k = 1, \ldots, n_b, \ i = 1, \ldots, N.$$

C. Multipatch Geometries

The parametrization (27) assumes that the geometry can be defined as the image of the unit square. In most practical situations, the geometry of the physical domain will differ topologically from a square. In these cases, we will represent the geometry by multiple patches, assuming that at the interfaces the patches match both parametrically and geometrically, that is, they have coincident knots and control points (see Fig. 4). With this approach, the continuity between patches is reduced to C^0, but high continuity can be maintained within each patch.

The way to deal with multiple patches in IGA is very simple. Since the boundary control points of two adjacent patches coincide at the interface, we also enforce the boundary degrees of freedom at that interface to coincide. This is very similar to what is done in FEM between adjacent elements. We notice that this approach only gives C^0 continuity of the solution between patches, and the refinement of one patch propagates to the adjacent one. It is also possible to obtain higher regularity than C^0 by enforcing some constraints on the first layer of internal knots, but these methods are beyond the scope of this paper. We refer the reader to [9] for more details on the subject.

VI. Numerical Result

The method has been implemented in MATLAB using the GeoPDEs toolbox[1] [18]. The integrals in the matrix entries (31)–(33) are approximated with Gaussian quadrature rules,

[1] Available at http://geopdes.sourceforge.net.

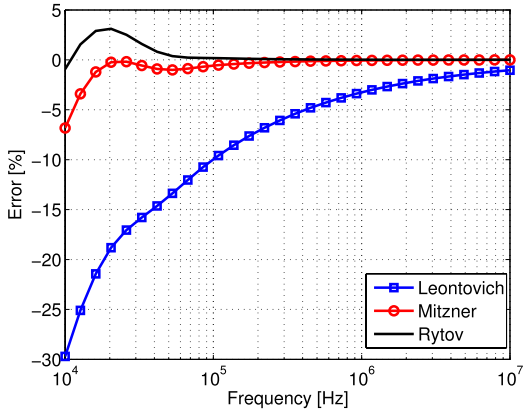

Fig. 5. Relative error in p.u.l. resistance for two circular copper cables of diameter equal to 2 mm. Distance between the centers of the conductors is 4 mm.

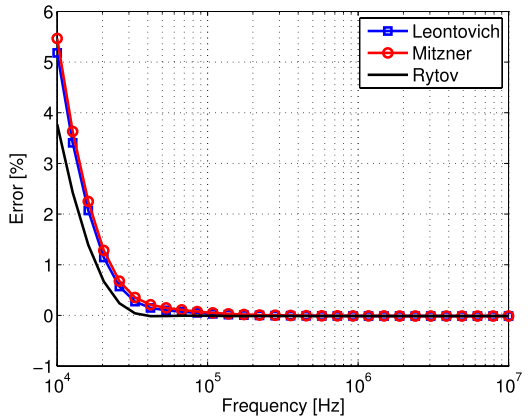

Fig. 6. Relative error in p.u.l. inductance for two circular copper cables of diameter equal to 2 mm. Distance between the centers of the conductors is 4 mm.

and standard algorithms from [16] are used to evaluate, at the quadrature points, the NURBS parametrization, the basis functions, and the derivatives of both. An alternative to these algorithms is the use of Bézier extraction, as it is described in [19].

To validate our implementation and to compare the obtained IGA results with the BEM computations presented in [1], we have chosen here the same test cases.

First of all the canonical problem of two parallel circular conductors is solved. Conductivity of each conductor is $\sigma = 5.8 \times 10^7$ S/m and diameter is 2 mm; distance between centers is 4 mm. The per-unit-length (p.u.l) series parameters are computed following the procedure described in [8]. The applied discretization is with NURBS of degree 3, the number of elements is equal to 3600 and the number of degrees of freedom is equal to 4761. The radius of the external boundary is $R = 0.04$ m. To compare our IGA results with those obtained with the BEM formulation in [1], Rytov's condition is implemented as a NtD SIBC as in (9), using the corresponding mixed formulation (25). The relative errors with respect to analytical results [20], shown in Figs. 5 and 6, are very close to those obtained in [1] and [8] using BEM, showing that they are due to the chosen SIBC and do not depend on the discretization

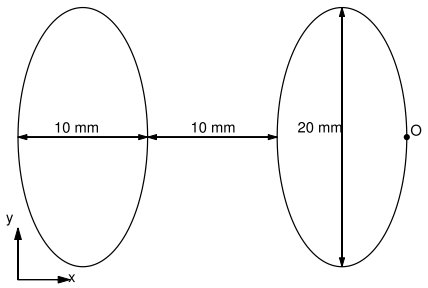

Fig. 7. Dimensions of the two elliptical conductors.

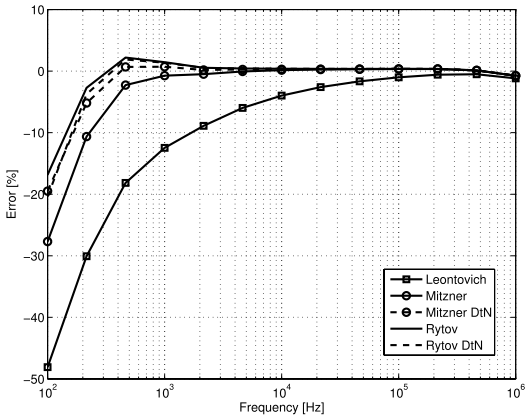

Fig. 8. Relative error, with respect to commercial FEM software results, in p.u.l. resistance for two elliptical copper cables.

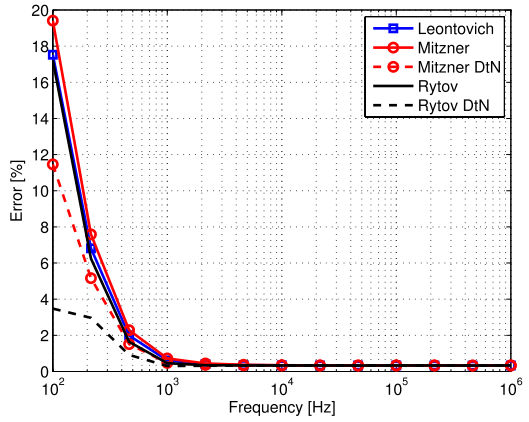

Fig. 9. Relative error, with respect to commercial FEM software results, in p.u.l. inductance for two elliptical copper cables.

technique. The DtN SIBCs (10)–(11) implemented with the formulation presented in Section IV-B give similar results and so are not reported in Figs. 5 and 6.

The second test case of two parallel elliptical conductors is then considered, with the dimensions given in Fig. 7 and the same electrical conductivities as in the circular conductors case. The numerical results for p.u.l. resistance and inductance are compared in Figs. 8 and 9 with those obtained with a commercial FEM software [21], which solves the problem including the discretization of (1) in the conductors, and that were reported in [1]. The degree of NURBS, the number of elements and of degrees of freedom is the same of the previous test case of two circular conductors. The radius of the external boundary is $R = 0.3$ m. As it can be noted the error does

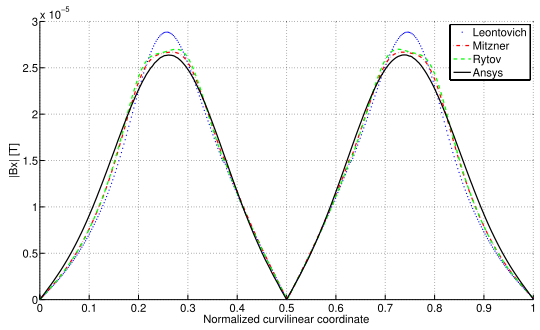

Fig. 10. Magnitude of the x-component of the magnetic field over the contour of the right conductor at 500 Hz. The origin of the curvilinear coordinate is at point O in Fig. 7.

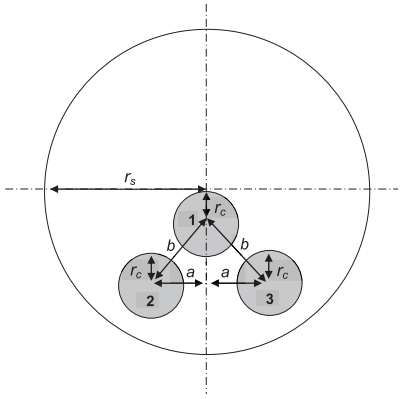

Fig. 11. Geometry of the three-phase power cable ($r_s = 100$ mm, $r_c = 17$ mm, $a = 1.5r_c$, $b = 3r_c$).

not converge exactly to zero, due to the finite size of the computational domain (as a matter of fact, the error converges to zero when the radius of the domain goes to infinity). We see from Fig. 9 that DtN conditions perform better in this example. This seems to be a problem-dependent feature, since the same behavior is not repeated in other tests. A comparison with the results obtained by the commercial FEM software is also carried out in terms of the magnetic field over the contour of the elliptical conductor (Fig. 10), at a frequency of 500 Hz. The high-order SIBCs give better results in this test case, but as the authors mention in [6], it is not guaranteed that raising the order of the SIBC will lead to better numerical results, as can be noted comparing the results for Mitzner and Rytov conditions.

Finally, to deal with a more realistic geometry, we have applied the method to the simulation of a three-phase cable with a shield (that we consider infinitely thick), with the same geometry of the example in [1] (see Fig. 11). The three phase conductors and the shield are supposed to be made of copper, with electrical conductivity $\sigma = 5.8 \times 10^7$ S/m and magnetic permeability $\mu = \mu_0$.

The discretization is done with NURBS of degree 3, the number of elements is equal to 15 300 and the number of degrees of freedom is equal to 17 758. In this case, the SIBC is also imposed on the shield, as explained in Remark 1. As can be noted from Figs. 12 and 13, there is a better convergence for high-order SIBCs, in particular for the resistance in Fig. 12,

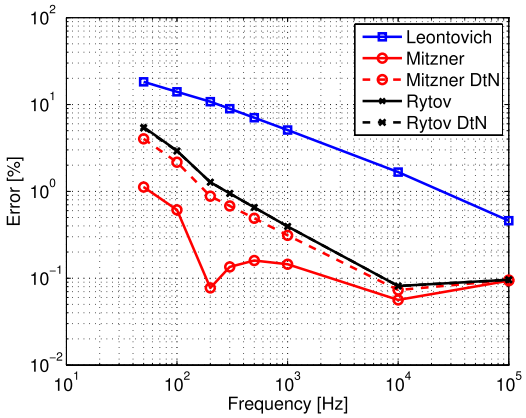

Fig. 12. Differences with commercial FEM software results in p.u.l. resistance of conductor 1.

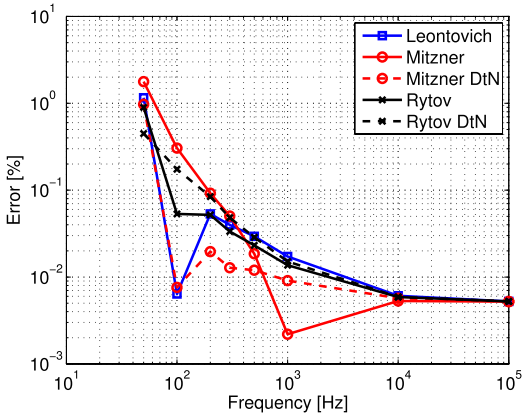

Fig. 13. Differences with commercial FEM software results in p.u.l. inductance of conductor 1.

although the behavior is not regular at the highest frequency (100 kHz), as the error does not go to zero. We attribute this effect to a lack of accuracy of the reference-adaptive FEM simulation, computed with 272 380 elements for this frequency. To improve the results we should use a higher number of finite elements, not obtainable with the computational resources at hand, showing in this way the relevant advantage of the use of SIBCs. The considered test case also shows that, even if all the approximations tend to the same results when frequency increases, it is not always the case that higher order SIBCs give lower errors, as it is seen in Fig. 13.

VII. Conclusion

High-order SIBCs are implemented in an isogeometric discretization of a 2-D variational formulation. Both NtD and DtN approaches are considered while introducing the impedance boundary conditions and the corresponding variational formulations are derived. In the case of the highest order Rytov's conditions, the NtD conditions require a mixed formulation with the use of more unknowns. The implementations are validated with the solution of three canonical cases, showing that all the approximation errors tend to be zero with increasing frequency, regardless of the kind and order of the impedance boundary conditions. Reference solutions are analytical or are obtained by a commercial finite element software. In some cases, the advantage of using high-order impedance boundary conditions can be appreciated in terms of accuracy. The present formulation can be extended to the vectorial 3-D case. In this case, one would apply the SIBCs presented in [5] and [7] and the discretization with isogeometric methods would require the use of the curl-conforming spline spaces introduced in [15], which are a generalization of edge finite elements to the isogeometric context.

References

[1] R. Vázquez, A. Buffa, and L. Di Rienzo, "NURBS-based BEM implementation of high-order surface impedance boundary conditions," *IEEE Trans. Magn.*, vol. 48, no. 12, pp. 4757–4766, Dec. 2012.

[2] M. A. Leontovich, "On the approximate boundary conditions for the electromagnetic field on the surface of well conducting bodies," in *Investigations of Radio Waves*, B. Vvedensky, Ed. Moscow, Russia: Academy, 1948, pp. 5–12.

[3] S. M. Rytov, "Calcul du skin-effet par la méthode des perturbations," *J. Phys. USSR*, vol. 2, no. 3, pp. 233–242, 1940.

[4] S. Yuferev and N. Ida, *Surface Impedance Boundary Conditions: A Comprehensive Approach*. Boca Raton, FL, USA: CRC, 2009.

[5] S. Yuferev and L. Di Rienzo, "Surface impedance boundary conditions in terms of various formalisms," *IEEE Trans. Magn.*, vol. 46, no. 9, pp. 3617–3628, Sep. 2010.

[6] H. Haddar, P. Joly, and H.-M. Nguyen, "Generalized impedance boundary conditions for scattering by strongly absorbing obstacles: The scalar case," *Math. Models Methods Appl. Sci.*, vol. 15, no. 8, pp. 1273–1300, 2005.

[7] H. Haddar, P. Joly, and H.-M. Nguyen, "Generalized impedance boundary conditions for scattering problems from strongly absorbing obstacles: The case of Maxwell's equations," *Math. Models Methods Appl. Sci.*, vol. 18, no. 10, pp. 1787–1827, Jan. 2008.

[8] L. Di Rienzo, S. Yuferev, and N. Ida, "Computation of the impedance matrix of multiconductor transmission lines using high-order surface impedance boundary conditions," *IEEE Trans. Electromagn. Compat.*, vol. 50, no. 4, pp. 974–984, Nov. 2008.

[9] J. A. Cottrell, T. J. R. Hughes, and Y. Bazilevs, *Isogeometric Analysis: Toward Integration of CAD and FEA*. New York, NY, USA: Wiley, 2009.

[10] J. Jin, *The Finite Element Method in Electromagnetics*, 2nd ed. New York, NY, USA: Wiley, 2002.

[11] L. Demkowicz, *Computing with Hp-Adaptive Finite Elements, Vol. 1: One and Two Dimensional Elliptic and Maxwell Problems* (Applied Mathematics and Nonlinear Science Series). Boca Raton, FL, USA: Chapman & Hall, 2007.

[12] F. Ihlenburg, *Finite Element Analysis of Acoustic Scattering* (Applied Mathematical Sciences), vol. 132. New York, NY, USA: Springer-Verlag, 1998.

[13] K. Schmidt and S. Tordeux, "High order transmission conditions for thin conductive sheets in magneto-quasistatics," *ESAIM Math. Model. Numer. Anal.*, vol. 45, no. 6, pp. 1115–1140, 2011.

[14] A. Darcherif, A. Raizer, J. Sakellaris, and G. Meunier, "On the use of the surface impedance concept in shielded and multiconductor cable characterization by the finite element method," *IEEE Trans. Magn.*, vol. 28, no. 2, pp. 1446–1449, Mar. 1992.

[15] A. Buffa, J. Rivas, G. Sangalli, and R. Vázquez, "Isogeometric discrete differential forms in three dimensions," *SIAM J. Numer. Anal.*, vol. 49, no. 2, pp. 818–844, Jan. 2011.

[16] L. Piegl and W. Tiller, *The Nurbs Book*. New York, NY, USA: Springer-Verlag, 1997.

[17] T. J. R. Hughes, J. A. Cottrell, and Y. Bazilevs, "Isogeometric analysis: CAD, finite elements, NURBS, exact geometry and mesh refinement," *Comput. Methods Appl. Mech. Eng.*, vol. 194, nos. 39–41, pp. 4135–4195, Oct. 2005.

[18] C. de Falco, A. Reali, and R. Vázquez, "GeoPDEs: A research tool for isogeometric analysis of PDEs," *Adv. Eng. Softw.*, vol. 42, no. 12, pp. 1020–1034, 2011.

[19] M. J. Borden, M. A. Scott, J. A. Evans, and T. J. R. Hughes, "Isogeometric finite element data structures based on Bézier extraction of NURBS," *Int. J. Numer. Methods Eng.*, vol. 87, nos. 1–5, pp. 15–47, Aug. 2010.

[20] V. Belevitch, "Theory of the proximity effect in multiwire cables—Part I," *Philips Res. Rep.*, vol. 32, no. 1, pp. 16–43, 1977.

[21] *ANSYS Maxwell 2D* [Online]. Available: http://www.ansys.com